

Part 2 of Supporting Information for:

ih-RIDME: a pulse EPR experiment to probe the heterogeneous nuclear environment

Sergei Kuzin*,¹ Victoriya N. Syryamina,² Mian Qi,³ Moritz Fischer,³ Miriam Hülsmann,³
Adelheid Godt,³ Gunnar Jeschke,¹ Maxim Yulikov¹

¹Department of Chemistry and Applied Biosciences, ETH Zurich, Vladimir-Prelog-Weg 2, 8093 Zurich, Switzerland

²Voevodsky Institute of Chemical Kinetics and Combustion, Novosibirsk 630090, Russia

³Faculty of Chemistry and Center for Molecular Materials (CM₂), Bielefeld University, Universitätsstraße 25, 33615 Bielefeld, Germany

Contents

| | |
|--|------------|
| S2 Approximation of the ih-RIDME kernel | S14 |
| S3 Tikhonov regularization | S15 |
| S4 EPR data on the model compound 1 | S16 |
| S4.1 Echo-detected field sweep EPR spectrum | S16 |
| S4.2 Hahn echo decay | S16 |
| S4.3 ih-RIDME data | S16 |
| S4.4 ih-RIDME fitting | S17 |
| S5 Molecular modeling | S20 |
| S5.1 General description | S20 |
| S5.2 Comparison of dihedral potentials | S20 |
| S5.3 Convergence of the dataset | S21 |
| S5.4 Comparison of the experimental and calculated $p(\sigma)$ | S21 |
| S6 ih-RIDME sequences | S24 |
| S6.1 Remote detection in 3p-RIDME | S24 |
| S6.2 ESEEM averaging in 4p-RIDME | S24 |
| S6.3 Comparison of the longitudinal factors | S25 |
| S6.4 Extraction of transverse factors $F(t)$ | S25 |

S2 Approximation of the ih-RIDME kernel

In Ref. [6], the diffusion equation for the magnetization spectrum $\mu(\omega, T)$ was solved via a series representation using Hermitian functions. Here, we decided to simplify this result by Gaussian fitting the ih-RIDME traces $R(t; T_{\text{mix}})$ calculated via the diffusion equation. We presented in Eq. (18) in the main text that the longitudinal dynamics is parametrized by the unitless parameters $\varepsilon = DT_{\text{mix}}/\sigma^3$ and σt . Thus, we calculated a family of ih-RIDME traces as functions of σt and parametrized by ε followed by fitting them with $\exp(-\alpha(\varepsilon)\sigma^2 t^2)$. The results are shown in Figure S2.1.

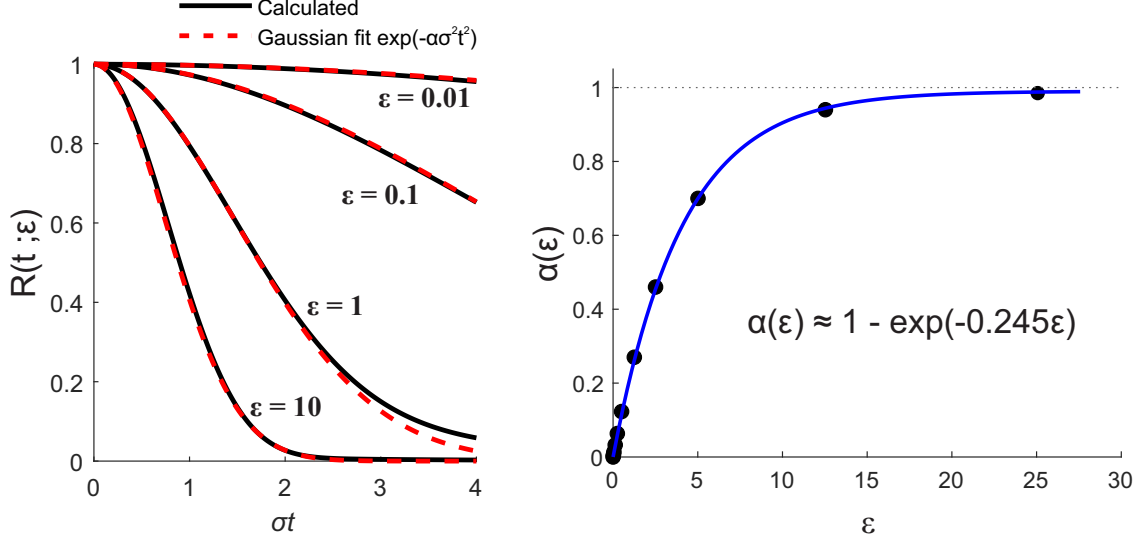


Figure S2.1: Left: examples of fitting of calculated time-domain RIDME traces by Gaussian function is a wide range of mixing times. Right: build-up of the extracted Gaussian curvature and its fitting

S3 Tikhonov regularization

Tikhonov regularization approach modifies the target minimization functional with a term $\|\mathbf{L}_n p\|$ where \mathbf{L}_n is a matrix of a discrete n^{th} derivative of the vector p . Traditionally, in PDS n equals 2. The general minimization problem in ih-RIDME with the smoothness penalty is then

$$p(\sigma) = \arg \min_{p \geq 0} \left\{ \sum_{i=1}^{M-1} w_i \left\| \frac{V(t; T_{\text{mix},i})}{V(t; T_{\text{mix,ref}})} - \frac{\int K(\sigma t; T_{\text{mix},i}) p(\sigma) d\sigma}{\int K(\sigma t; T_{\text{mix,ref}}) p(\sigma) d\sigma} \right\| + \alpha^2 \|\mathbf{L}_2 p\| \right\}. \quad (\text{S3.1})$$

The regularization parameter α^2 tunes the weight of the smoothness penalty. In the top plot of Figure S3.1, we show fitted distributions of the noised dataset (NSR 0.05, see Section 4.2.2 in the main text) with different values of the regularization parameter.

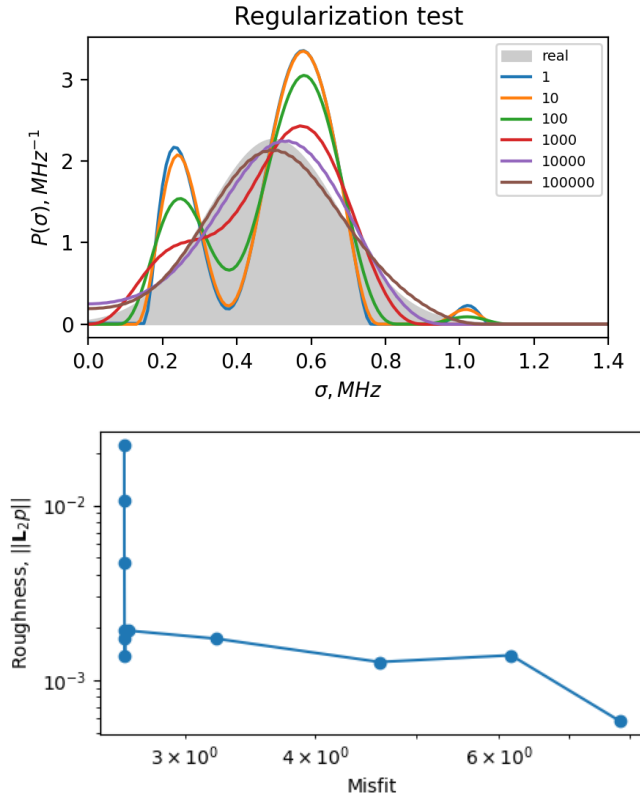


Figure S3.1: Top: fitted distributions $p(\sigma)$ for a noised dataset with different regularization parameter. Numbers in the legend correspond to the value of α^2 . Bottom: the corresponding L-curve.

The selection of the regularization parameter can be made based on a traditional L-curve criterion. The L-curve for the case under consideration is presented in Figure S3.1 (bottom). It features a distinct L-shape. The value in the corner of the L-curve corresponds to the brown distribution in the top panel.

S4 EPR data on the model compound **1**

S4.1 Echo-detected field sweep EPR spectrum

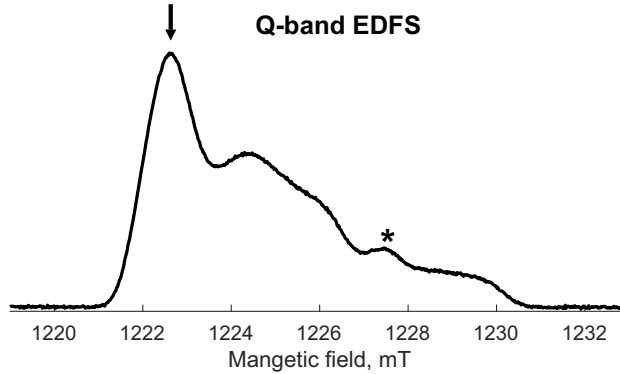


Figure S4.1: Q-band ($\nu_{mw} = 34.5$ GHz) echo-detected field sweep EPR spectrum of model compound **1** in a perdeuterated water-glycerol solvent. The arrow indicates the field position for the pulse EPR measurements. The pulses were set to $t_{\pi/2} = 12$ ns and $t_{\pi} = 24$ ns. The asterisk marks the radical defect in the quartz capillary.

S4.2 Hahn echo decay

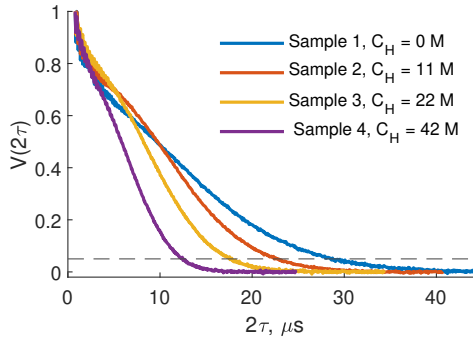


Figure S4.2: Normalized Hahn echo decay traces of the model compound **1** in partially deuterated water/glycerol. See Table 1 in the main text for details on the isotope composition. The measurements were done at Q band at 50 K. Dash line displays 5% of the initial intensity.

| Sample | $C_H(\text{solvent})$ | $t_{0.05}, \mu s$ |
|----------|-----------------------|-------------------|
| 1 | 0 | 28.5 |
| 2 | 11.4 | 22.6 |
| 3 | 22.1 | 17.6 |
| 4 | 41.7 | 12.4 |

Table S4.1: Times of the Hahn echo decay to 5% of the initial amplitude of model compound **1** in water/glycerol solutions with different protonation degrees.

S4.3 ih-RIDME data

The normalized raw data as well as the reference-divided traces are presented in Figure S4.3.

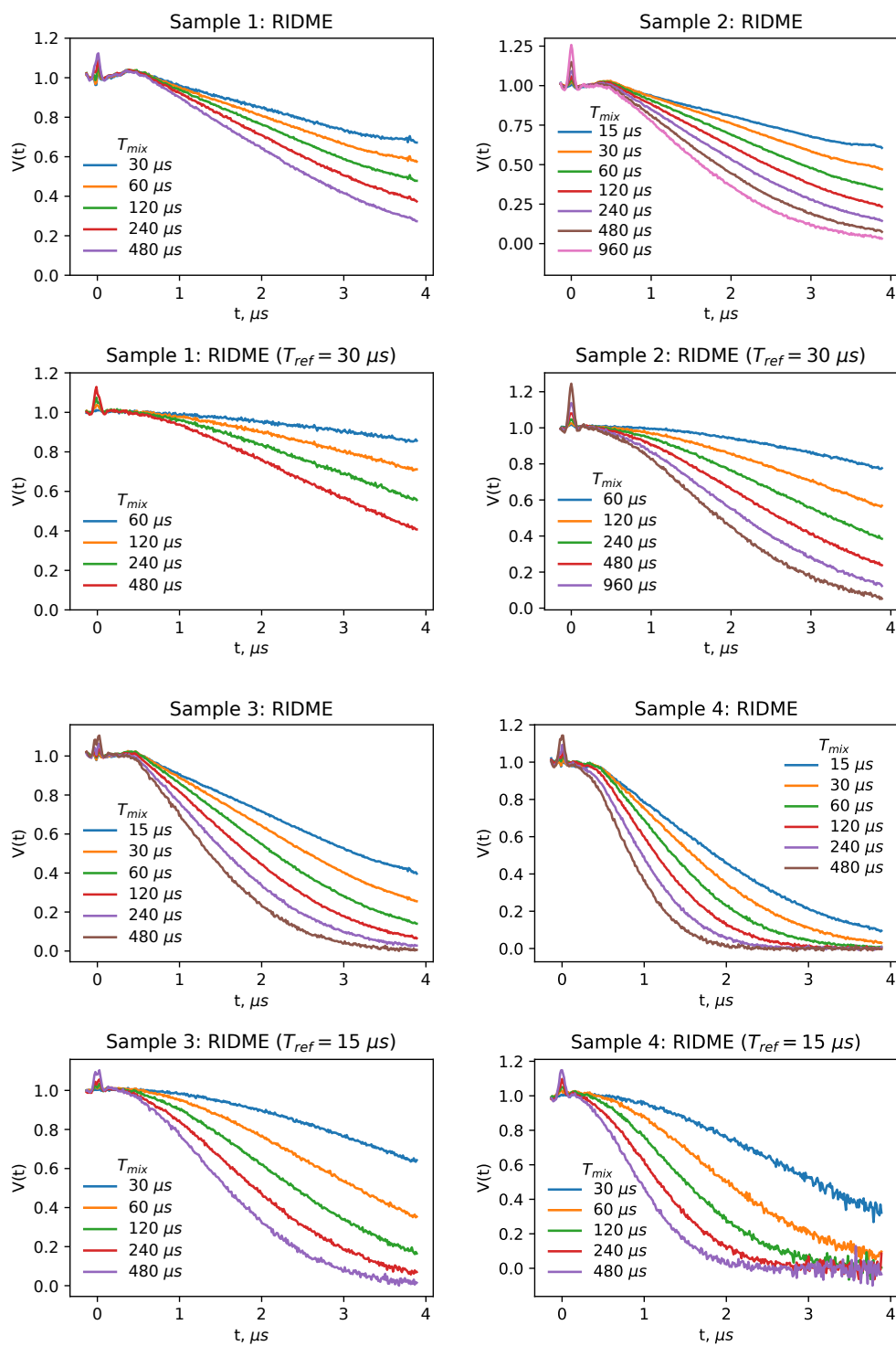


Figure S4.3: Normalized ih-RIDME traces and reference-divided ih-RIDME traces for four solutions of model compound **1**. See Table 1 in the main text for solvent composition.

S4.4 ih-RIDME fitting

The fitting of reference-divided ih-RIDME traces was done with an approximate kernel

$$K(\sigma t; T_{\text{mix}}) = \exp(-(\alpha(T_{\text{mix}}) + \beta)\sigma^2 t^2) \quad (\text{S4.1})$$

with

$$\alpha(T_{\text{mix}}) = 1 - \exp\left(-0.245 \frac{D}{\sigma^3} T_{\text{mix}}\right). \quad (\text{S4.2})$$

The visual comparison of reference-divided experimental and fitted data is given in Figure S4.4.

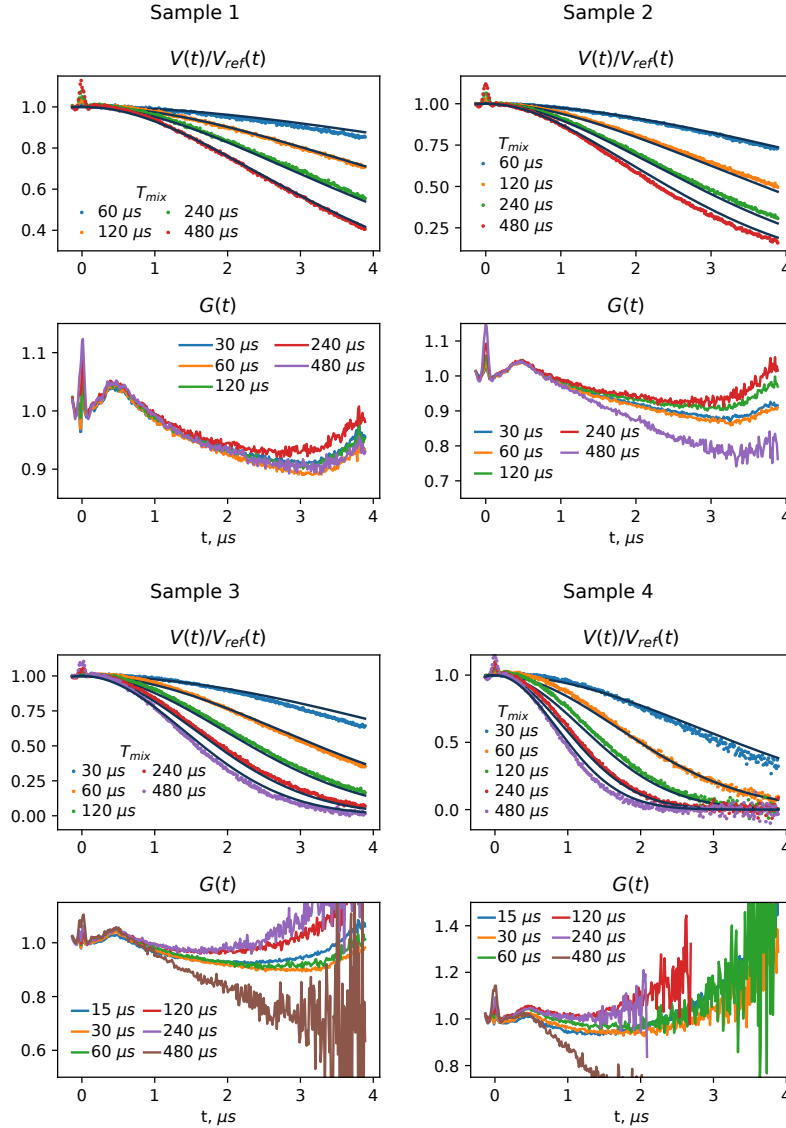


Figure S4.4: ih-RIDME data fits (black lines) and the residual factor $G(t)$ for a model compound **1** in different solvents. See Table 1 in the main text for details.

We analyzed the factor residuals of the undivided experimental data

$$G(t; T_{\text{mix}}) = \frac{V_{\text{exp}}(t; T_{\text{mix}})}{V_{\text{fit}}(t; T_{\text{mix}})} \quad (\text{S4.3})$$

where $V_{\text{exp}}(t; T_{\text{mix}})$ are the experimental traces and $V_{\text{fit}}(t; T_{\text{mix}})$ are the traces computed for the optimized proton density distribution $P_{\text{opt}}(\sigma)$

$$V_{\text{fit}}(t; T_{\text{mix}}) = \int_{\sigma_{\text{min}}}^{\sigma_{\text{max}}} K(\sigma t; T_{\text{mix}}) P_{\text{opt}}(\sigma) d\sigma. \quad (\text{S4.4})$$

We found that the residuals are almost independent of mixing time and have characteristic roof-shaped features at $t \approx d_1$. The position of these features in the RIDME time axis slightly deviates from d_1 due to the used ^2H -ESEEM averaging protocol[5] that increments the first interpulse delay from d_1 to $d_1 + 0.256 \mu\text{s}$. A similar feature was observed in copper-nitroxide biradicals[7], however, it was not assigned to the presence of copper.

In general, the features found are not critical for the processing of ih-RIDME data. Due to T_{mix} -independence, the factor $G(t)$ is removed from the reference-divided dataset and does not interfere with the approximation (S4.1). This is, however, an obstacle towards the fitting of unreferenced data, therefore, this effect should be investigated further.

S5 Molecular modeling

S5.1 General description

The molecule was constructed from blocks with variable dihedral angles by a home-written MATLAB script. The blocks, which are shown in blue in Figure S5.1, were independently created in Avogadro software [3], optimized with MMFF94s force field [2], and further merged. The O-C-C-O dihedral angles α , β , and γ were chosen from optimized potentials for liquid simulations (further denoted as OPLS) or modified OPLS profiles, which were taken from Ref. [4] and fitted by the sum of Gaussian distributions. The dihedral angles δ (C-C-O-C), ε (H-C-C-H), ζ (C-N-C-C) and κ (O-C-C-C) were chosen from the profile for methyl groups in ethane ([1]) and fitted by the sum of Gaussian distributions. The dihedral angle probabilities are shown in Figure S5.2. The dihedral angle η (C₂₃ - N - C₁ - C₆), the angle θ (C₂ - C₃ - O - C), the angle ι (C₁₀ - C₁₁ - O - C and C₁₃ - C₁₄ - O - C) and the angle λ (C₂₁ - C₂₀ - O - C) were canonical angles (0° and 180°). The μ (C₅ - C₄ - C₉ - C₁₄) and ν (C₁₃ - C₁₂ - C₁₇ - C₂₂) angles were canonical angles (0°). In a separate try, the low-amplitude libration near the canonical values for angles η , θ , ι , μ and ν was introduced. The distribution of libration amplitudes was taken Gaussian:

$$U(\alpha) = \frac{1}{\sqrt{2\pi}|\Delta\alpha|} \exp\left(-\frac{(\alpha - \alpha_{\text{canonic}})^2}{2|\Delta\alpha|^2}\right) \quad (\text{S5.1})$$

with $\Delta\alpha = 7^\circ$ for angles η , θ , and ι , and 5° for μ and ν angles. The results obtained with this modification are further referred to as “with libration”.

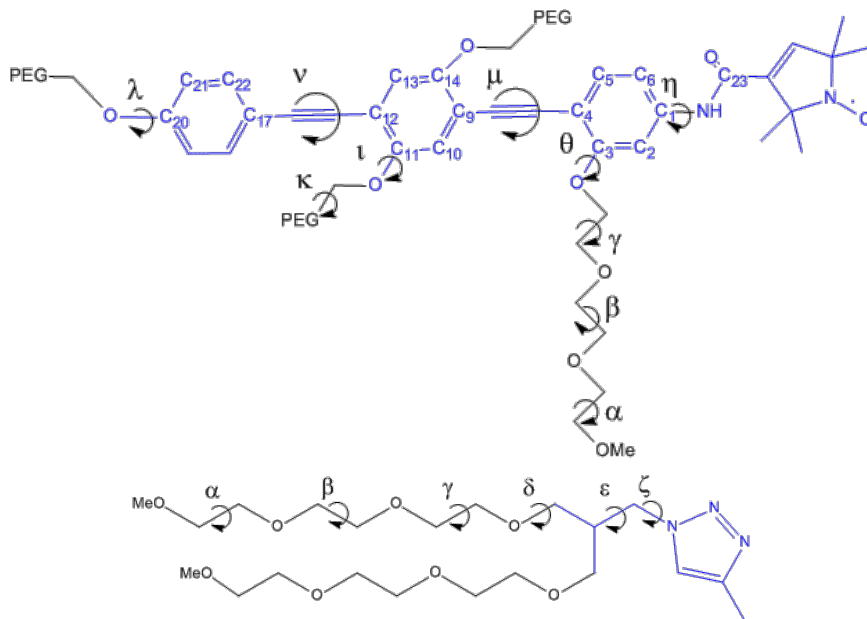


Figure S5.1: The molecular structure of model compound **1** and definition of variable dihedral angles.

S5.2 Comparison of dihedral potentials

The ensembles were generated with four combinations: unmodified or modified OPLS dihedral potentials and without or with angle libration. We found that the obtained ensembles have rather similar characteristics. As an example, we show in Figure S5.4 the correlation plot for the maximal distance between the electron spin and the farthestmost proton in a given conformer and the gyration

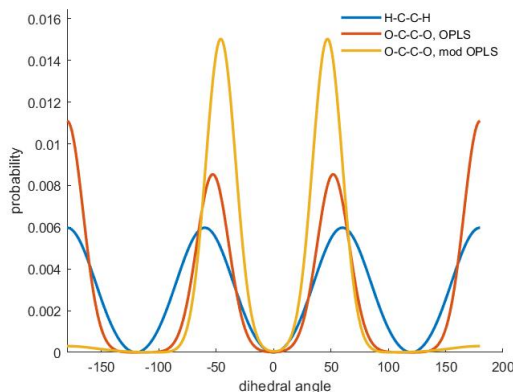


Figure S5.2: Dihedral angle probabilities for H-C-C-H in ethane (blue line) and O-C-C-O in OPLS (orange line) and modified OPLS (“mod OPLS”, yellow line) potentials.

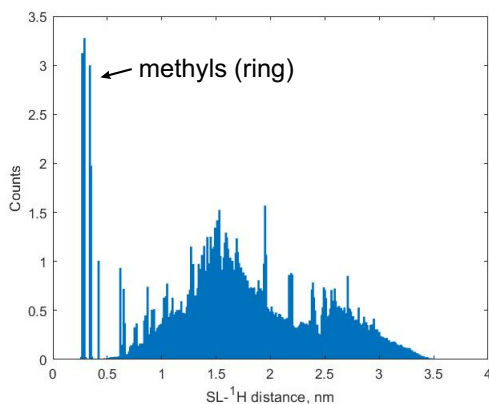


Figure S5.3: Spin-label- ^1H distance distribution function for dataset constructed with OPLS profile and canonic η , θ , ι , λ , μ and ν angles.

radius of the same conformer. The first descriptor estimates the size of a molecule along the longest dimension. The second descriptor reflects the compactness of a molecule. Besides the slight correlation of these two values in the conformational ensemble, we observe that the four settings of the ensemble generation substantially overlap with each other. Therefore, we cannot give a preference to any of the models from the analysis of the ensemble.

S5.3 Convergence of the dataset

We worked with a conformational ensemble of 1500 conformers. We tested that this number is sufficient by computing the distribution $p_n(\sigma)$ for subsets of variable sizes $n < 1500$ and comparing them with the $p(\sigma) = p_{1500}(\sigma)$ computed for the full set. As a result, we obtained a convergence plot in Figure S5.5. This curve has a steep feature at the beginning and reaches a shallow plateau after approximately 500 conformers. Further increase of the subset size has a weak impact on the convergence rate. Nonetheless, 1500 conformers of model compound **1** was still a computationally feasible size for a regular computer.

S5.4 Comparison of the experimental and calculated $p(\sigma)$

We compared the normalized distributions $p(\sigma)$ calculated from the generated ensembles with the experimental distribution of the model compound **1** in the fully deuterated solvent (Sample 1

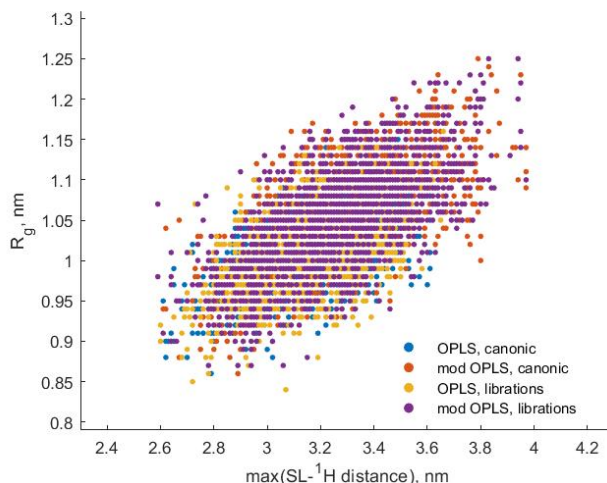


Figure S5.4: Correlation of the distance from the unpaired electron to the farthest proton of a conformer ($\max(\text{SL}^{-1}\text{H distance})$) and the molecule’s gyration radius (R_g) sampled over the generated conformational ensemble assuming OPLS or modified OPLS model with and without librations.

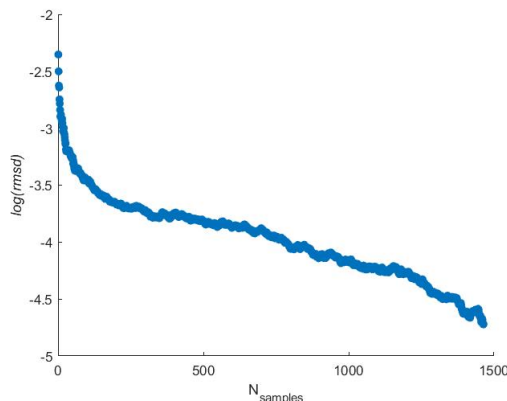


Figure S5.5: The rmsd between local proton densities averaged over the dataset with 1500 conformers, and for various numbers of conformers. Results are shown for the canonical OPLS dataset with a cutoff radius of 1.55 nm.

in the main text). Upon the comparison, we introduced a cutoff radius r_{cut} which models the protons that are excluded from the spectral diffusion and, thus, are not observable in ih-RIDME. The cutoff radius was scanned in the range of 0.5-2.0 nm. Since the generated ensembles in four different models are close, the calculated distributions are also close and we discuss them together.

The comparison with the experiment was based on the calculation of rmsd, mean, width and skewness of the distributions (Figure S5.6). The rmsd criterion and the comparison of the mean values suggested that the best agreement with the experiment is achieved at $r_{\text{cut}} = 1.55$ nm. The calculated distributions with $r_{\text{cut}} = 1.55$ nm are narrower than the experimental result (panel C in Figure S5.6). This may be related to the overestimation of the distribution width from the ih-RIDME fitting. In addition, the experimental distribution is characterized by a stronger skewness than those calculated. These findings may also indicate that the unrestrained conformational ensemble of the model compound **1** is not an accurate enough model. In this scenario, the ih-RIDME data would be useful to refine the confirmation ensemble.

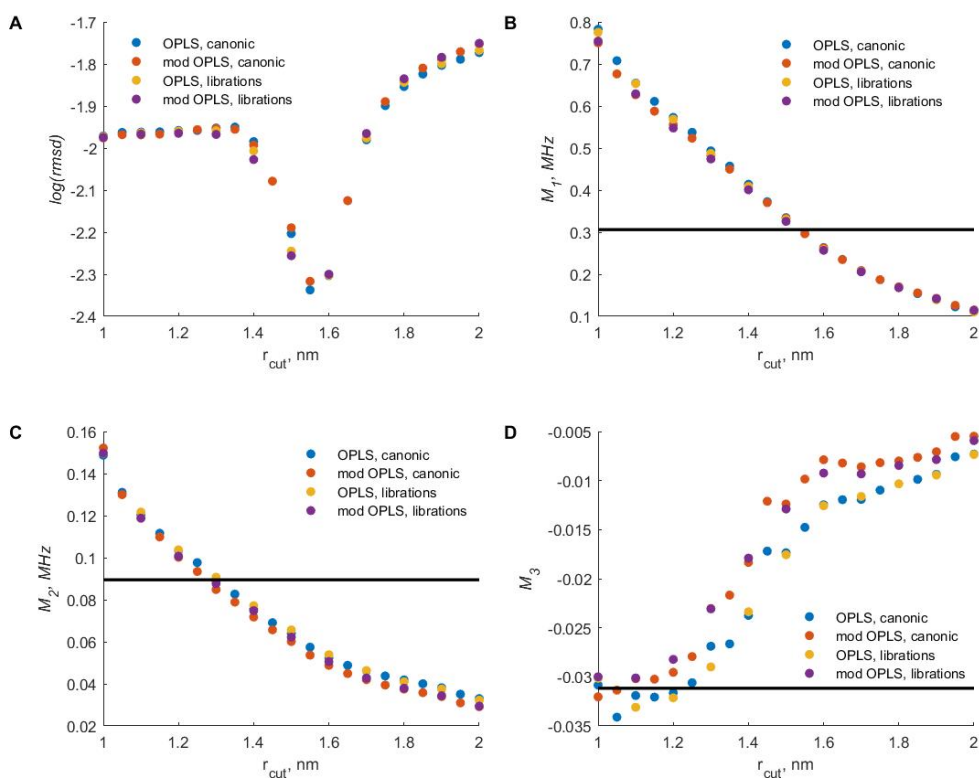


Figure S5.6: A. The rmsd for local proton density from experimental data and calculated from datasets constructed with various OPLS profiles at different cutoff radii. The mean ($M_1 = \mu_1$, panel B), the width ($M_2 = \mu_2^{1/2}$, panel C), and the skewness ($M_3 = \mu_3/\mu_2^{3/2}$, panel D) of local proton density distribution, calculated from experimental RIDME traces (black line), and for datasets constructed with various OPLS profiles at different cutoff radius (coloured circles). All parameters were estimated in the range of σ -axis 0 – 0.48 MHz.

S6 ih-RIDME sequences

S6.1 Remote detection in 3p-RIDME

A direct comparison of 3p-RIDME and 3pRD-RIDME (three-pulse with remote detection) traces in Figure S6.1 shows that the remote detection does not introduce data distortion to the 3p-RIDME data.

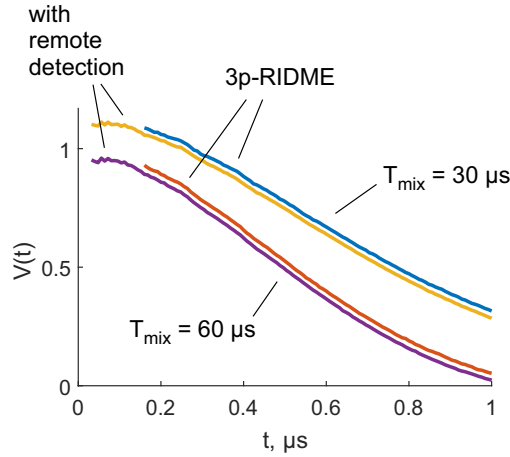


Figure S6.1: Comparison of 3p-RIDME traces with those recorded using the remote detection block (3pRD-RIDME). The latter traces have lower dead time (32 ns) and their shape perfectly overlaps with 3p-RIDME traces demonstrating that remote detection does not introduce data distortion. The measurements were done for TEMPO in H₂O/H₈-glycerol at 50 K at Q band.

S6.2 ESEEM averaging in 4p-RIDME

The ESEEM averaging in 4p-RIDME can be achieved by incrementing the length of delay d_1 . In the example in Figure S6.2, the ²H-ESEEM in Q band ($1/\nu_I(^2\text{H}) \approx 123$ ns) was averaged by stepping d_1 in 16 ns 8 times.

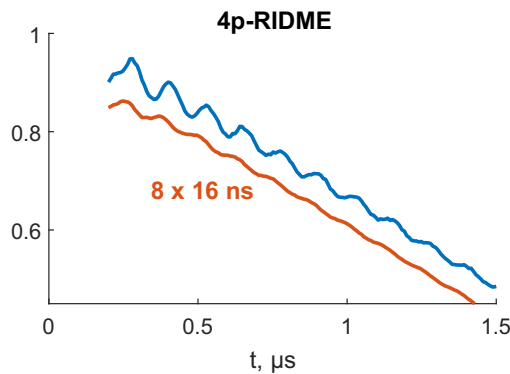


Figure S6.2: 4p-RIDME traces of TEMPO in partially deuterated water/glycerol matrix at Q band. Blue line: without ²H-ESEEM averaging protocol. Orange line: with averaging protocol (d_1 delay is incremented 8 times with a step of 16 ns). The orange curve is shifted vertically downwards for better visibility.

S6.3 Comparison of the longitudinal factors

The 5p-RIDME, 3pRD-RIDME and 5pVT-RIDME traces were measured at Q band with a solution of TEMPO radical in water/glycerol solvent (protonation degree 51%). The trace shapes differ in the time domain (see Figure 11 in the main text). After the division by the reference trace, the datasets show a good extent of similarity. In a homogeneous solution, the trace division eliminates the transverse factor in the ih-RIDME traces. The good shape match of the divided traces means that the longitudinal factors in the three versions of the HYSDEMON experiment are very close and the differences in the undivided data are determined by the transverse factors. This confirms the signal model for an ih-RIDME (HYSDEMON) experiment.

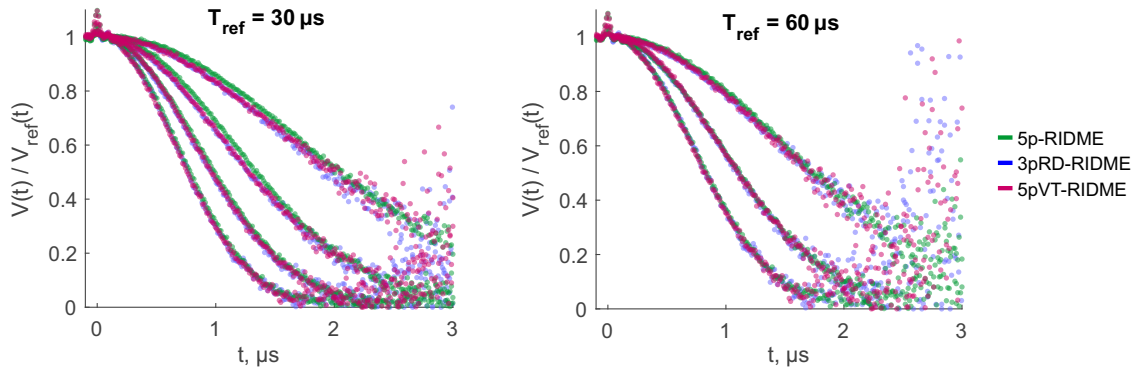


Figure S6.3: Series of ih-RIDME traces (5p-RIDME - green, 3pRD-RIDME - blue, 5pVT-RIDME - magenta) divided by a reference trace with $T_{\text{mix}} = 30 \mu\text{s}$ (left panel) and $60 \mu\text{s}$ (right panel).

S6.4 Extraction of transverse factors $F(t)$

The transverse factors in 3p-RIDME and 5pVT-RIDME traces ($F_{3p}(t)$, respectively, $F_{5p}(t)$; see Figure 11 in the main text) were extracted using the relation

$$F_{\bullet}(t) = \frac{V_{\bullet}(t; T_{\text{mix}})}{R(t; T_{\text{mix}})} \quad (\text{S6.1})$$

where $V_{\bullet}(t; T_{\text{mix}})$ are the experimental traces (the bullet sign replaces 3p or 5p) at different mixing times and $R(t; T_{\text{mix}})$ are longitudinal factors computed according to (see Eqs. (18) and (19) in the main text)

$$R(t; T_{\text{mix}}) = \vec{c}_0^T \exp(-i\hat{R}\sigma t) \exp\left(\frac{D}{\sigma^3} \hat{\Gamma} T_{\text{mix}}\right) \exp(i\hat{R}\sigma t) \vec{c}_0. \quad (\text{S6.2})$$

The parameters for simulation were taken from Ref. [6] and were $D/\sigma^3 = 18 \text{ ms}^{-1}$ and $\sigma = 1.23 \text{ MHz}$.

References

- [1] Rodolfo O Esquivel, Shubin Liu, Juan Carlos Angulo, Jesús S Dehesa, Juan Antolín, and Moyocoyani Molina-Espíritu. Fisher information and steric effect: Study of the internal rotation barrier of ethane. *J. Phys. Chem. A*, 115(17):4406–4415, 2011.
- [2] Thomas A Halgren. MMFF VI. MMFF94s option for energy minimization studies. *J. Comput. Chem.*, 20(7):720–729, 1999.
- [3] Marcus D Hanwell, Donald E Curtis, David C Lonie, Tim Vandermeersch, Eva Zurek, and Geoffrey R Hutchison. Avogadro: an advanced semantic chemical editor, visualization, and analysis platform. *J. Cheminf.*, 4:1–17, 2012.
- [4] Markus M Hoffmann, Matthew D Too, Nathaniel A Paddock, Robin Horstmann, Sebastian Kloth, Michael Vogel, and Gerd Buntkowsky. On the behavior of the ethylene glycol components of polydisperse polyethylene glycol peg200. *J. Phys. Chem. B*, 127(5):1178–1196, 2023.
- [5] Katharina Keller, Andrin Doll, Mian Qi, Adelheid Godt, Gunnar Jeschke, and Maxim Yulikov. Averaging of nuclear modulation artefacts in ridme experiments. *J. Magn. Reson.*, 272:108–113, 2016.
- [6] Sergei Kuzin, Gunnar Jeschke, and Maxim Yulikov. Diffusion equation for the longitudinal spectral diffusion: the case of the RIDME experiment. *Phys. Chem. Chem. Phys.*, 24(38):23517–23531, 2022.
- [7] Irina Ritsch, Henrik Hintz, Gunnar Jeschke, Adelheid Godt, and Maxim Yulikov. Improving the accuracy of Cu (II)–nitroxide RIDME in the presence of orientation correlation in water-soluble Cu (II)–nitroxide rulers. *Phys. Chem. Chem. Phys.*, 21(19):9810–9830, 2019.